WO_3 ADDITION, CRYSTAL PHASE EVOLUTION AND PROPERTIES OF Y_2O_3-DOPED ALN CERAMICS

#HYUNHO SHIN, SANG-OK YOON, SHIN KIM, INJOON HWANG

Department of Materials Engineering, Gangneung-Wonju National University, Gangneung, Gangwon-do 210-702, Republic of Korea

#E-mail: hshin@gwnu.ac.kr

Submitted March 7, 2014; accepted July 25, 2014

Keywords: Aluminum nitride, WO_3, Optical reflectance, Thermal conductivity, Dielectric properties

The effect of WO_3 addition on the densification, phase evolution, and properties of Y_2O_3-doped AlN ceramics sintered at 1800°C for 3 h was investigated. The total amount of oxides added was 4.5 wt. %. In all of the compositions investigated, $YAlO_3$ and $Y_4Al_2O_9$ were observed as the secondary phases. When WO_3 was added, W_2B was also identified. As the quantity of WO_3 increased, the amount of $YAlO_3$ and W_2B increased and that of $Y_4Al_2O_9$ decreased. However, the sinterability and thermal conductivity of the sintered body were not influenced much. The optical reflectance decreased from 25 to approximately 10 % in the visible-light regime, by the formation of W_2B. For the sintered body with composition 3.5 Y_2O_3–1.0 WO_3–95.5 AlN, the thermal conductivity, the elastic modulus, and the Poisson ratio were 134 $Wm^{-1}K^{-1}$, 368 GPa and 0.196, respectively; and the dielectric constant and loss tangent at the resonant frequency of 8.25 GHz were 8.60 and 0.003, respectively.

INTRODUCTION

The thermal conductivity of single crystal AlN (320 $Wm^{-1}K^{-1}$) is sixteen times higher than that of Al_2O_3 at room temperature: almost equal to that of BeO (99.5 % pure) at 150°C [1]. Using various aids, sintered AlN ceramics demonstrate a reasonably high thermal conductivity ranging from 70 to 270 $Wm^{-1}K^{-1}$. Since AlN requires a fairly high temperature to achieve full density due to its highly covalent bonding, extensive investigations on the sintering additives have been carried out. In general, rare earth oxides and alkaline earth oxides have been effective for the densification of AlN ceramics [2-4]. In particular, lithium compounds such as $LiYO_2$ are efficient at lowering the sintering temperature [5], and $Ca_3Al_2O_6$ has been adopted for improving their translucency [6].

In addition to high thermal conductivity, AlN possesses other useful properties (i.e., as high electrical resistivity, high dielectric strength, low dielectric constant, and a thermal expansion coefficient matching that of silicon). Such attributes make AlN attractive for microelectronics applications; it is used as a substrate for multichip modules and packaging materials for integrated circuits (ICs) [7]. In order to prevent photoconductive errors in semiconductor chips, and to hide the interior wiring of a multilayer package, the materials used for IC packaging are usually required to be black or opaque. In this regard, Kasori *et al.* [8], who sintered compacts of mixed powder of AlN with 0.3 wt. % of transition-metal compounds, and 3 wt. % of Y_2O_3, reported that most of the added transition-metal compounds turned AlN ceramics black or gray without significant deterioration of their thermal conductivity, sinterability, and other (electrical and mechanical) properties. They also reported that, when WO_3 was added, the total transmittance of the specimen at the wavelength 800 nm was less than 2 % while that of the reference specimen without transition-metal compound was 57 %. This result indicates that WO_3 is efficient for producing darkened AlN ceramics, but only a few studies have investigated the effect from adding WO_3 on the properties of AlN ceramics [7, 8]. The purpose of this study is to systematically examine the effect of the varying substitution of WO_3 for Y_2O_3 on the properties of AlN ceramics.

EXPERIMENTAL

Raw powders of AlN (H grade, Tokuyama Co. Ltd., Japan, 0.85 wt. % oxygen), Y_2O_3 (Purity 4N, High Purity Chemicals Co. Ltd, Japan), and WO_3 (Purity 3N, High Purity Chemicals Co. Ltd, Japan) were mixed to prepare a series with the composition (4.5-x) Y_2O_3–x WO_3–95.5 AlN (where x = 0; 0.25; 0.50; 0.75 and 1.0). A 20 g batch of each composition was ball-milled using ZrO_2 balls in ethanol medium in a polyethylene-based container for 5 h, followed by drying in an oven, uniaxial pressing at 100 MPa to form a disk shape (diameter 20 mm), and cold isostatic pressing at 200 MPa. The disk-

shaped specimens were transferred to a BN-coated graphite crucible, heat treated at 400°C for 2 h, and sintered at 1800°C for 3 h in a graphite furnace. The heat treatment and sintering were carried out in flowing N_2 gas (1 l/min) at 1 atm.

The crystalline phases of sintered specimens were identified using a powder X-ray diffractometer (Model X'pert PRO MPD, PANalytical, Ea Almelo, Netherlands). The Rietveld refinement was carried out using the RIETAN-FP program package [9]. The microstructure of sintered specimens was characterized using a field emission scanning electron microscope (FESEM, Model SU-70, Hitachi, Tokyo, Japan). The compositional analysis was performed using energy-dispersive spectroscopy (EDS, Model Pegasus XM4, EDAX Inc., Mahwah, NJ, USA). After mirror-polishing their surface, the optical reflectance of the sintered specimens was measured using a spectrophotometer (Model V650, JASCO International Co., Ltd., Tokyo, Japan), in the wavelength range from 200 to 800 nm. The apparent density of the sintered specimens was measured by the Archimedes principle using ethanol medium. The elastic modulus and Poisson ratio were determined by the ultrasonic pulse-echo technique (Model UT340, UTEX Scientific Instruments Inc., Mississauga, Ontario, Canada). The microwave dielectric properties of the sintered disk specimens were measured using a network analyzer (E5071C ENA, 100 kHz-8.5 GHz; Agilent Technologies, Palo Alto, CA, USA) with the Hakki–Coleman fixture configuration [10].

RESULTS AND DISCUSSION

Evolution of crystalline phases and microstructure

The powder X-ray diffraction patterns of the Y_2O_3 and WO_3-doped AlN ceramics sintered at 1800°C for 3 h are shown in Figure 1. AlN with a hexagonal structure was identified as the main phase in all the compositions investigated. $YAlO_3$ with an orthorhombic structure (ICDD number 33-0041 [11]) and $Y_4Al_2O_9$ with a monoclinic one (ICDD number 34-0368 [12]) were observed as the secondary phases when only Y_2O_3 was added (x = 0 in the (4.5-x) Y_2O_3–x WO_3–95.5 AlN system). It is known that Y_2O_3 reacts with the oxide layer of AlN powder (i.e., Al_2O_3) and, at high temperatures, forms the liquid phase composed of yttrium-aluminum oxides, which promotes the liquid-phase sintering of AlN [1-8].

Ueno [13] reported that, cubic $Y_3Al_5O_{12}$ (one of the compounds in the Y_2O_3–Al_2O_3 system [14]), formed in the composition range of 0.5 - 3 wt. % Y_2O_3. Virkar et al. [15] pointed out the possibility of the decomposition of $YAlO_3$ into $Y_3Al_5O_{12}$ and $Y_4Al_2O_9$ during cooling. In this investigation (Figure 1), however, $Y_3Al_5O_{12}$ was not detected. The amount of Y_2O_3 in this study (3.5 - 4.5 wt.%, corresponding to x = 1.0 and 0, respectively) is considered too great to form $Y_3Al_5O_{12}$. Thus, the decomposition of $YAlO_3$ might have not occurred in this study.

In the WO_3-added specimens (x = 0.25 - 1.0), in addition to $YAlO_3$ and $Y_4Al_2O_9$, tungsten boride (W_2B) with a tetragonal structure (ICDD number 25-0990 [16]) was identified (Figures 1b-e. Among unidentified peaks, those at two theta values between 25.6 and 39.6 degrees were related to the phase(s) containing tungsten since the peak intensity increased as the amount of WO_3 increased. The peak at 31.8 degree was not related to the tungsten because this peak was observed in all specimens from x = 0.

In order to determine the relative proportion of the crystalline phases, the Rietveld refinement was carried out by neglecting the traces of unidentified phase(s). The result for the specimen at x = 1.0 is shown in Figure 2 as an example. In this figure, dotted and solid lines indicate the measured and simulated XRD patterns, respectively,

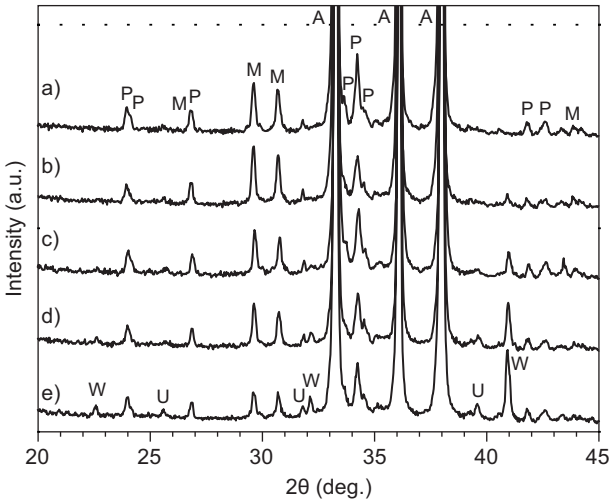

Figure 1. Powder XRD patterns of Y_2O_3 and WO_3-doped AlN ceramics sintered at 1800°C for 3 h: a) x = 0, b) x = 0.25, c) x = 0.50, d) x = 0.75 and e) x = 1.0 (A - AlN, P - $YAlO_3$, M - $Y_4Al_2O_9$, W - W_2B and U - unidentified phase).

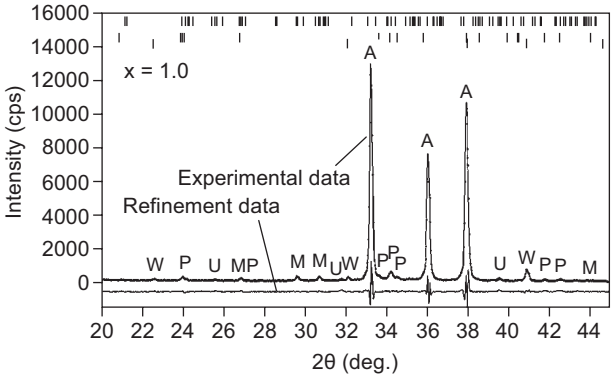

Figure 2. Result of Rietveld refinement for Y_2O_3 and WO_3-doped AlN ceramics when x = 1.0 (A - AlN, P - $YAlO_3$, M - $Y_4Al_2O_9$, W - W_2B and U - unidentified phase).

and the bottom curve denotes the difference between the experiment and the simulation. The values of R_{wp}, the weighted profile R-factor, and S, the goodness-of-fit indicator ($S = R_{wp}/R_{exp}$, where R_{exp} is the expected R-factor) are 16.3 - 16.8 and 3.1 - 3.2, respectively. Figure 3 shows the quantitative amount of crystalline phases determined by the Rietveld refinement as a function of x in the (4.5-x) Y_2O_3-x WO_3-95.5 AlN system. The phase quantity of AlN was calculated to be 96.2 - 97.3 wt. %. The phase quantity of $Y_4Al_2O_9$ was inversely proportional to that of AlN, indicating that its formation was directly related to AlN decomposition. As x increased (i.e. the amount of Y_2O_3 decreased), the phase quantities of $YAlO_3$ and W_2B increased monotonically.

The microstructure when x = 0.50 in the (4.5-x) Y_2O_3–x WO_3–95.5 AlN system is shown in Figure 4a. The bright-colored phases are composed of elements (Y and W) heavier than the AlN grain, and thus are interpreted to be the secondary phases, $YAlO_3$, $Y_4Al_2O_9$, and W_2B. The areas marked by arrows in Figure 4a are likely W_2B because the EDS result at the spot position (Figure 4b) turned out to be rich in tungsten (not shown). The grain-size distribution of the W_2B particles was wide (10 nm to ca. 1 mm), indicating that the formation path is complicated (as for W [8]). The shape of W_2B particles was almost spherical, which may be associated with the reaction path for its formation; dissolution-precipitation or vapor-phase reaction, as suggested in next subsection.

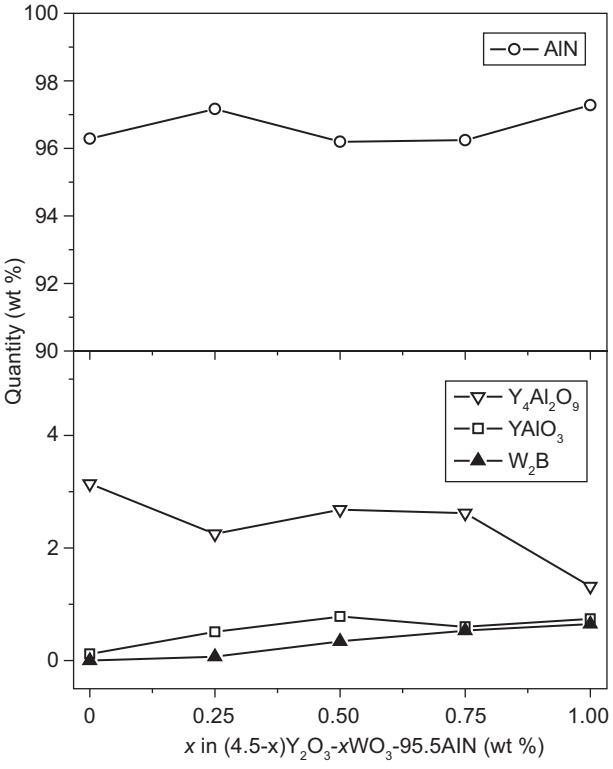

Figure 3. Relative amount of crystalline phases determined by the Rietveld refinement as a function of x in the (4.5-x) Y_2O_3-xWO_3-95.5AlN system.

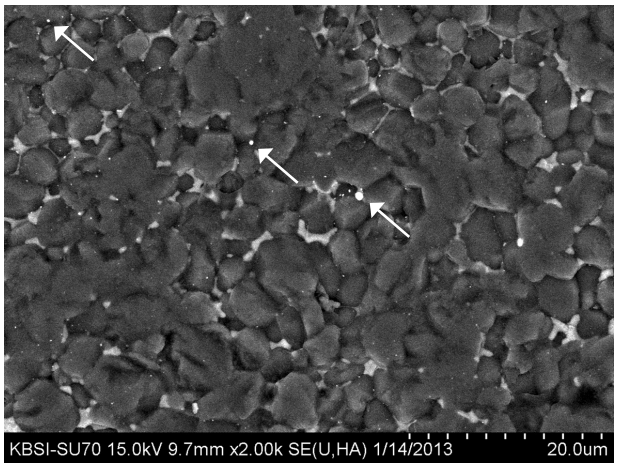

a)

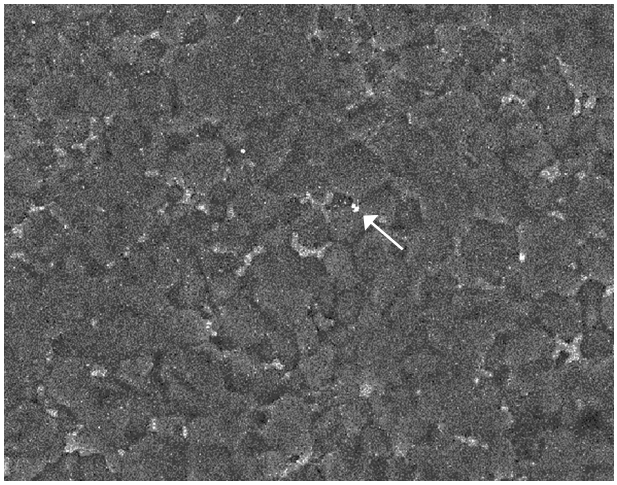

b)

Figure 4. FE-SEM micrograph for the a) Y_2O_3 and WO_3-doped AlN specimen when x = 0.5 and b) EDS spot position on W_2B.

Reaction path to form W_2B

Since W_2B formed in a reducing atmosphere (graphite furnace with graphite heating elements and felt) in this study, it may be informative to review the existing studies relevant to the formation of W_2B. The source of the boron may be BN, coated on the graphite crucible, because BN is the only material containing boron in this study and also in that of Kasori et al [8], who also reported the formation of WB_2. By noting this point, the behavior of BN and WO_3 is focused as follows.

The vapor pressure of BN increased from ca. 10^{-8} atm at 1300°C to ca. 10^{-5} atm at 1600°C [17], based on this, the vapor pressure of BN was roughly estimated to be approximately 10^{-3} atm at 1800°C, which may be sufficient to provide the boron for formation of W_2B, at the sintering temperature of 1800°C. Sata and Urano [17] reported that vaporized BN decomposed into boron (solid) and nitrogen (gas) at this temperature (BN (g) → B (s) + ½ N_2 (g)).

As for the behavior of WO_3, two characteristic features are noted. First, it reacts with a trace of Al_2O_3 on the surface of AlN at above 1200°C to form a W–Al–O liquid according to the phase diagram of the Al_2O_3–WO_3 system [18]. As the temperature increases, Y_2O_3 is reasonably anticipated to react with the W–Al–O liquid to form a new Y–W–Al–O liquid. This liquid promotes the densification of AlN ceramics and then, during cooling, various secondary phases such as $YAlO_3$ and $Y_4Al_2O_9$ precipitate [19]. Second, at temperatures above 1660°C, the WO_3 component vaporizes selectively from the Y_2O_3-WO_3 binary compounds [20-21]. A significant vaporization of WO_3 in a nitrogen stream in a carbon tube furnace was also reported [22].

With the knowledge of the behavior of BN and WO_3 outlined above, two plausible scenarios of the WB_2-forming reaction path can be conceived. First, the BN vapor dissolves into the Y–W–Al–O liquid to form a B–N–Y–W–Al–O liquid which facilitates densification, followed by the precipitation of AlN, Y–Al–O secondary phases, and WB_2 during cooling. In Kasori et al. [8], tungsten-rich spheres (possibly WB_2) with approximately 100 nm were detected not only in the intra-granular region but also inside the AlN grain. Their observation supports the scenario of the formation of WB_2 (also AlN) from the B–N–Y–Al–W–O liquid.

Second, note that the borothermic reduction of WO_3 is much more exothermic than the reaction between tungsten and boron. Actually, it is the major process in the self-sustaining combustion of the WO_3–B–W system [23]. Thus, it is justifiably anticipated that sublimed WO_3, either from the residual WO_3 which does not join the W–Al–O liquid or from the liquid itself, is reduced to form W under the presence of B from decomposed BN [17]. The next step, the reaction of W with B to form WB_2, is possible and has been proven experimentally; (1) When powder mixtures of tungsten and BN were heat-treated in Ar gas, W_2B formed among the compounds of tungsten boride [17]. (2) When a multi-layer circuit board of AlN with a circuit pattern of tungsten was sintered in a BN container, BN diffused into the tungsten of the circuit conductor and formed W_2B [24]. (3) By the reaction of a BN-W powder mixture, W_2B and WB were produced in the vapor phase (above 1500°C) [25].

Properties of the sintered specimen

The optical reflectance spectra of Y_2O_3 and WO_3-doped AlN ceramics, in the ultraviolet and visible-light wavelength ranges, are shown in Figure 5. The reflectance of the specimen at x = 0 (Figure 5a) was approximately 25 % in the visible-light wavelengths (400 - 700 nm). By the substitution of WO_3 for Y_2O_3, (i.e., by the formation of W_2B), the reflectance decreased drastically; At x = 0.25, it was less than approximately 10 percent at visible-light wavelengths and decreased further with x (Figure 5b-e). Above the wavelength of 450 nm, the reflectance spectra of the WO_3-added specimens was roughly flat (i.e., achromatic; specimens were black).

The linear shrinkage and apparent density, as well as the thermal, elastic, and dielectric properties of the Y_2O_3 and WO_3-codoped AlN ceramics, are summarized in Table 1. When no WO_3 was added (x = 0), the linear

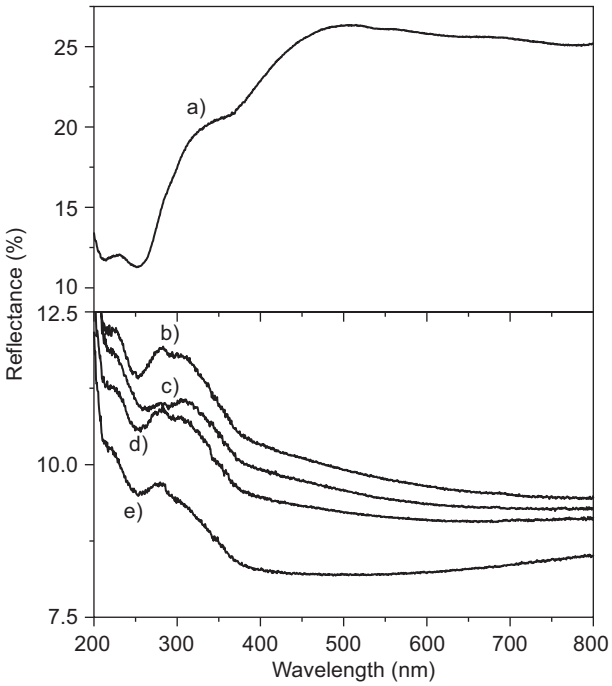

Figure 5. Reflectance spectra of Y_2O_3 and WO_3-doped AlN ceramics sintered at 1800°C for 3 h; a) x = 0, b) 0.25, c) 0.50, d) 0.75, and e) 1.0.

Table 1. Linear shrinkage, bulk density, and properties of Y_2O_3 and WO_3-doped AlN ceramics.

x	Linear shrinkage (%)	Apparent density (g/cm^3)	Elastic modulus (GPa)	Poisson ratio	Thermal conductivity ($Wm^{-1}K^{-1}$)	Dielectric constant	Loss tangent/10^{-3}	Resonant frequency (GHz)
0	20.8	3.34	362	0.146	137	8.63	2.65	8.27
0.25	20.3	3.36	353	0.176	136	8.59	3.22	8.31
0.50	20.7	3.36	366	0.163	135	8.57	3.01	8.23
0.75	20.7	3.36	364	0.160	130	8.60	3.79	8.29
1.0	20.6	3.37	368	0.196	134	8.60	3.06	8.25

shrinkage of the specimen was 20.8 %, whereas that of the specimens with W_2B was between 20.3 and 20.7 %. This result appears to indicate that the formation of W_2B does not inhibit the sinterability of the AlN ceramics. A similar result was also found in the case of the substitution of Ga_2O_3 for Y_2O_3 in the Y_2O_3 and Ga_2O_3 co-doped AlN ceramics [26]. The apparent density of the specimen was 3.34 - 3.37 g/cm^3, which is higher than that of AlN (3.26 g/cm^3) due to the formation of secondary phases with higher densities (5.35; 4.52; and 17.09 g/cm^3 for $YAlO_3$, $Y_4Al_2O_9$, and W_2B, respectively [11, 12, 16]).

The thermal conductivity of the specimen at x = 0 was 137 $Wm^{-1}K^{-1}$ (Table 1). This value was not influenced much by the addition of WO_3, but a slightly decreasing trend can be claimed from Table 1. The elastic modulus of the specimen with x = 0 was 362 GPa: a value higher than those of polycrystalline AlN ceramics (308 - 322 GPa, [27-29]) but lower than that of single crystal AlN (374 GPa [30]). As the amount of W_2B increased, there was no apparent change in the elastic modulus. Each specimen with W_2B exhibited an elastic modulus of 364 - 368 GPa except for the specimen with x = 0.25 which showed a slightly lower value (reason presently unknown). Although the elastic modulus of W_2B is high (387.8 - 431 GPa [31-32]), the elastic modulus was not much increased, possibly because the amount of W_2B was less than 1 %. The Poisson ratio of the specimen at x = 0 was 0.146, which is lower than that of polycrystalline AlN ceramics (0.179 [27] or 0.245 [28]). The Poisson ratio of the specimens with W_2B was higher than 0.146.

The dielectric constant of the specimens was approximately 8.60 without regard to the formation of WB_2. The presence of W_2B did not influence the dielectric constant much. The loss tangent of the specimen without W_2B (x = 0) was 0.00265. Savrun and Nguyen [33] reported that there was a wide range in the loss tangent for AlN ceramics (between 0.0005 and 0.01) depending on the processing technique and raw materials. The loss tangent of the specimens with W_2B was slightly larger than that without W_2B.

CONCLUSION

The effect from the addition of WO_3 on the densification, phase evolution, optical reflectance, elastic modulus, dielectric constant, and loss tangent of Y_2O_3-doped AlN ceramics sintered at 1800ºC for 3 h was investigated. The total amount of oxides (i.e., sintering additives) was 4.5 wt. %. When only Y_2O_3 was added, in addition to the main crystalline phase of AlN, secondary phases were observed in the forms of $YAlO_3$ (with an orthorhombic perovskite structure) and $Y_4Al_2O_9$ (with a monoclinic structure). As the amount of WO_3 substituted for Y_2O_3 increased, the phase quantity of $YAlO_3$ increased, whereas that of $Y_4Al_2O_9$ decreased. For specimens to which WO_3 was added, tungsten boride (W_2B) with a tetragonal structure was also identified, and its phase quantity increased with amount of WO_3 added. The range of the grain size of W_2B was fairly large (from 10 nm to ca. 1 mm). W_2B might be precipitated from a liquid phase composed of Y–Al–W–B–O–N, formed by the dissolution of Y_2O_3, AlN, and BN vapor into A–W–O liquid, or by the reaction between boron and tungsten, where boron and tungsten were provided from the decomposition of BN vapor and the borothermic reduction of WO_3 by boron, respectively.

Sinterability was not inhibited by the presence of W_2B. The linear shrinkage and the apparent density were above 20 % and 3.34 - 3.37 g/cm^3, respectively. After formation of W_2B, the optical reflectance decreased drastically from 25 to less than approximately 10 % at visible light wavelengths; the color of the specimen changed from gray or dark gray to black. As the amount of W_2B was increased, the Poisson ratio showed a trend of slight increase while there was no apparent change in the elastic modulus. The dielectric constant was not changed much by the formation of W_2B but the loss tangent increased slightly. For 3.5 Y_2O_3–1.0 WO_3––95.5 AlN, the thermal conductivity, the elastic modulus, and the Poisson ratio were 134 $Wm^{-1}K^{-1}$, 368 GPa and 0.196, respectively, while the dielectric constant and the loss tangent at the resonant frequency of 8.25 GHz were 8.60 and 0.003, respectively.

Acknowledgments

This study was financially supported by the Human Resource Training Project for Regional Innovation, funded by the Ministry of Education, Science, and Technology (MEST) through the National Research Foundation (NRF) of Korea. The authors appreciate the technical assistance of Mr. Sangwoo Bang.

REFERENCES

1. Medraj M., Baik Y., Thompson W.T., Drew R.A.L.: J. Mater. Process. Tech. *161,* 415 (2005).
2. Komeya K., Inoue H., Tsuge A.: Yogyo-Kyokai-Shi *89,* 330 (1981).
3. Komeya K., Tsuge A., Inoue H., Ohta H.: J. Mater. Sci. Lett. *1,* 325 (1982).
4. Kranzmann A., Greil P., Petzow G.: Sci. Sinter. *20,* 135 (1988).
5. Watari K., Hwang H.J., Toriyama M., Kanzaki S.: J. Am. Ceram. Soc. *79*, 1979 (1996).
6. Honma T., Kuroki Y., Okamoto T., Takata M., Kanechika Y., Azuma M., Taniguchi H.: Ceram. Int. *34,* 943 (2008).
7. Nagai Y., Lai G.: J. Ceram. Soc. Jpn. *106,* 12 (1998).
8. Kasori M., Ueno F., Tsuge A.: J. Am. Ceram. Soc. *77,* 1991 (1994).
9. Izumi F., Momma K.: Solid State Phenom. *130*, 15 (2007).

10. Hakki B.W., Coleman P.D. : IRE Trans. Microwave Theory & Tech. *8,* 402 (1960).
11. Powder Diffraction File 33-0041, International Center for Diffraction Data (ICDD).
12. Powder Diffraction File 34-0368, International Center for Diffraction Data (ICDD).
13. F. Ueno, in: *Electric Refractory Materials*, p. 691-714, Eds. Y. Kumashiro, Marcel Dekker, Inc., New York, 2000.
14. Toropov N.A., Bondar I.A., Galadhov F.Y., Nikogosyan K.S., Vinogradova N.V.: Russ. Chem. Bull. *13,* 1076 (1964).
15. Virkar A.V., Jackson T.B., Cutler R.A., J. Am. Ceram. Soc. *72*, 2031 (1989).
16. Powder Diffraction File 25-0990, International Center for Diffraction Data (ICDD).
17. Sata T., Urano T.: Yogyo-Kyokai-Shi *78,* 27 (1970).
18. Waring J.L.: J. Am. Ceram. Soc. *48*, 493 (1965).
19. Kuribayashi K., Yoshimura M., Ohta T., Sata T.: J. Am. Ceram. Soc. *63,* 644 (1980).
20. Kuribayashi K., Sata T.: Bull. Chem. Soc. Jpn. *50,* 2932 (1977).
21. Kuribayashi K. Sata T.: Yogyo-Kyokai-Shi *87,* 321 (1979).
22. M. Miyake, A. Hara: J. Jpn. Soc. Powder Powder Metall. *26*, 16 (1979).
23. Yeh C.L., Wang H.J.: Ceram. Int. *37,* 2597 (2011).
24. Makihara H., Omote K., Kamehara N., Tsukada M.: U.S. Patent No. 5 683 529; 1997.
25. Borisova A.L., Martsenyuk I.S.: Sov. Powder Metall. Met. Ceram. *14,* 822 (1975).
26. Shin H., Yoon S.O., Kim S., Bang S.: Sci. Sinter. in press (2014).
27. Gerlich D., Dole S.L., Slack G.A.: J. Phys. Chem. Solids *47,* 437 (1986).
28. Boch P., Glandus J.C., Jarrige J., Lecompte J.P., Mexmain J.: Ceram. Int. *8,* 34 (1982).
29. Ruh R., Zangvil A., Barlowe J.: Am. Ceram. Soc. Bull. *64,* 1368 (1985).
30. Yonenaga I., Shima T., Sluiter M.H.F.: Jpn. J. Appl. Phys. *41,* 4620 (2002).
31. Xiao B., Feng J., Zhou C.T., Xie X.J., Cheng Y.H., Zhou R.: Physica B *405,* 1274 (2010).
32. Liang Y., Zhong Z., Zhang W.: Comput. Mater. Sci. *68,* 222 (2013).
33. Savrun E., Nguyen V. in: Proc. of the 7th IEEE International Vacuum Electronics Conference, p. 35-36, Ed. B. Fickett, Institute of Electrical and Electronics Engineers (IEEE), 2006.